Journal of Biomolecular NMR, **17:** 195–202, 2000.
KLUWER/ESCOM

[^{15}N,^{1}H]/[^{13}C,^{1}H]-TROSY for simultaneous detection of backbone ^{15}N–^{1}H, aromatic ^{13}C–^{1}H and side-chain ^{15}N–^{1}H$_2$ correlations in large proteins

Konstantin Pervushin, Daniel Braun, César Fernández & Kurt Wüthrich*
Institut für Molekularbiologie und Biophysik, Eidgenössische Technische Hochschule Hönggerberg, CH-8093 Zürich, Switzerland

Received 16 February 2000; Accepted 6 April 2000

Key words: isotope-labeled proteins, NMR structure determination, transverse relaxation-optimized spectroscopy, TROSY

Abstract

This paper describes a [^{15}N,^{1}H]/[^{13}C,^{1}H]-TROSY experiment for the simultaneous acquisition of the heteronuclear chemical shift correlations of backbone amide ^{15}N–^{1}H groups, side chain ^{15}N–^{1}H$_2$ groups and aromatic ^{13}C–^{1}H groups in otherwise highly deuterated proteins. The ^{15}N–^{1}H and ^{13}C–^{1}H correlations are extracted from two subspectra of the same data set, thus preventing possible spectral overlap of aromatic and amide protons in the ^{1}H dimension. The side-chain ^{15}N–^{1}H$_2$ groups, which are suppressed in conventional [^{15}N,^{1}H)-TROSY, are observed with high sensitivity in the ^{15}N–^{1}H subspectrum. [^{15}N,^{1}H]/[^{13}C,^{1}H]-TROSY was used as the heteronuclear correlation block in a 3D [^{1}H,^{1}H]-NOESY-[^{15}N,^{1}H]/[^{13}C,^{1}H]-TROSY experiment with the membrane protein OmpA reconstituted in detergent micelles of molecular weight 80 000 Da, which enabled the detection of numerous NOEs between backbone amide protons and both aromatic protons and side chain ^{15}N–^{1}H$_2$ groups.

Abbreviations: rf, radio-frequency; 2D, two-dimensional; FID, free induction decay; DD, dipole–dipole; CSA, chemical shift anisotropy; COSY, correlation spectroscopy; TROSY, transverse relaxation-optimized spectroscopy; PFG, pulsed field gradient; S/N, signal-to-noise ratio; OmpA, N-terminal transmembrane domain with residues 1–171 of the *E. coli* outer membrane protein A; DHPC,1,2-dicaproyl-sN-glycero-3-phosphocholine; OmpA/DHPC, OmpA reconstituted in DHPC micelles; ^{13}C^{R}, aromatic ring carbon; ^{1}H^{R}, aromatic ring proton; ^{1}H^{N}, amide proton; DSS, 2,2-dimethyl-2-silapentane-5-sulfonate, sodium salt.

Introduction

With the use of ^{13}C-labeled glucose as the sole carbon source and ^{15}NH$_4$Cl as the sole nitrogen source in minimal media containing 99% ^{2}H$_2$O, ^{13}C,^{15}N-labeled proteins are obtained that are highly deuterated at all aliphatic carbons, and between 50% and 99% protonated at the aromatic rings of Phe, Tyr, Trp and His (Gardner and Kay, 1998). With this labeling pattern it is attractive to combine [^{15}N,^{1}H]-TROSY (Pervushin et al., 1997, 1998b) and [^{13}C^{R},^{1}H^{R}]-TROSY (Meissner and Sørensen, 1999a,b; Pervushin et al., 1998a) in a single measurement. This paper describes a novel TROSY-type heteronuclear correlation element that enables just that, i.e. simultaneous recording of backbone ^{15}N–^{1}H, side-chain ^{15}N–^{1}H$_2$ and aromatic ^{13}C–^{1}H correlations with little compromise of sensitivity and resolution for each of the individual correlations, as it was previously also suggested for conventional NMR experiments (Farmer, 1991; Boelens et al., 1994; Farmer and Mueller, 1994; Pascal et al., 1994; Sattler et al., 1995; Slijper et al., 1996). Further use of this approach in more complex NMR experiments is a special attraction, for example, as a building block in 3D heteronuclear-resolved NOESY experiments to enable simultaneous detection of ^{1}H^{N}-^{1}H^{N}, ^{1}H^{R}–^{1}H^{R} and ^{1}H^{N}-^{1}H^{R} NOEs.

*To whom correspondence should be addressed. Fax: +41-1-6331151.

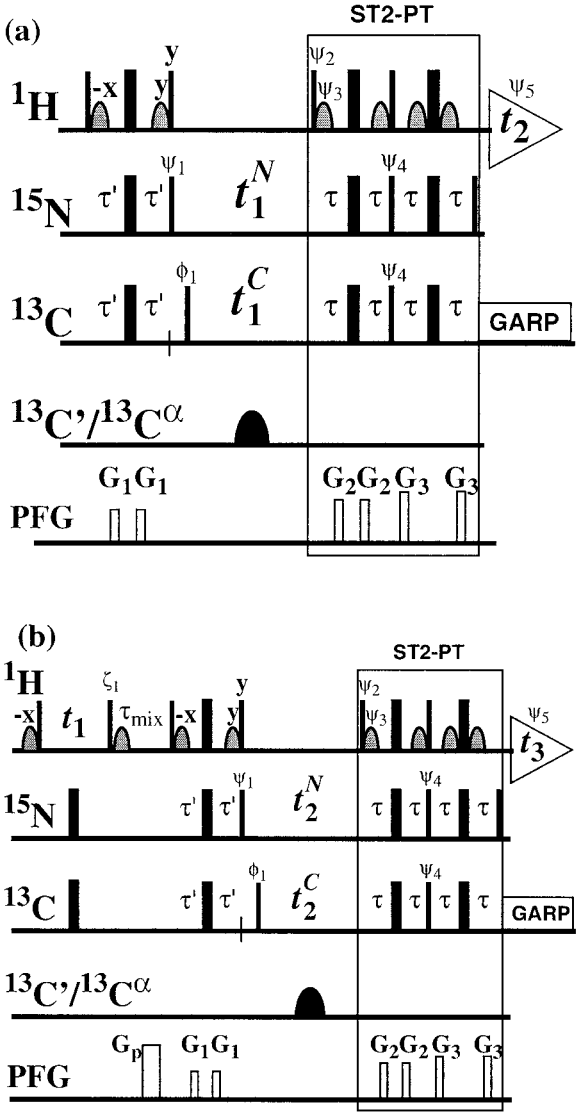

Figure 1. (a) Experimental scheme for 2D [^{15}N,^{1}H]/[^{13}C,^{1}H]-TROSY, using detection by single transition-to-single transition polarization transfer (box identified with ST2-PT). On the lines marked ^{1}H, ^{15}N and ^{13}C, narrow and wide bars stand for non-selective 90° and 180° radio-frequency pulses, with the carriers placed at 4.7, 119 and 130 ppm, respectively. The line ^{13}C′/^{13}C$^\alpha$ contains a two-band-selective inversion I-BURP-2 pulse (Geen and Freeman, 1991) with a duration of 3 ms, which is applied for all t_1 values that are sufficiently long to accommodate the pulse. The line marked PFG indicates the pulsed magnetic field gradients, which are all applied along the z-axis: G_1, amplitude 30 G/cm, duration 1 ms; G_2, 40 G/cm, 1 ms; G_3, 48 G/cm, 1 ms. To prevent splitting of the ^{13}C–^{1}H resonances along the ω_1(^{13}C) dimension due to the $^1J_{CC}$ couplings (~55 Hz), the ^{13}C chemical shift evolution delay, t_1^C, is chosen as $t_1^C = t_1^N/(t_{1max}^N * 2^1J_{CC})$. To obtain ^{15}N–^{1}H and ^{13}C^R–^{1}H^R subspectra, two data sets, I and II, are recorded with different phase cycling. I: Ψ_1 = {y, −y, −x, x}; Φ_1 = {y, −y, −x, x}; Ψ_2 = {−y}, Ψ_3 = {y}, Ψ_4 = {−y}, Ψ_5(receiver) = {y, −y, −x, x}, x on all other pulses. II: same as I, except that Φ_1 is inverted to {−y, y, x, −x}. The sum, I + II, results in the [^{15}N,^{1}H]-TROSY subspectrum, and I−II gives [^{13}C,^{1}H]-TROSY. To obtain a complex interferogram, a pair of data sets is recorded for each t_1 delay, with identical phases Φ_1 and Ψ_5, Ψ_1 = {y, −y, x, −x}, Ψ_2 = {y}, Ψ_3 = {−y} and Ψ_4 = {y}. ^{13}C GARP broadband decoupling with $\gamma B_1 = 3$ kHz is used during signal acquisition. One thus obtains a 2D [^{15}N,^{1}H]-correlation spectrum that contains only the most slowly relaxing component of the 2D ^{15}N–^{1}H and ^{15}N–^{1}H$_2$ multiplets (Pervushin et al., 1998b), and a 2D [^{13}C,^{1}H]-correlation spectrum that contains only the more slowly relaxing component of the ^{13}C doublet (Pervushin et al., 1998a). The data are processed as described by Kay et al. (1992). Water saturation is minimized by keeping the water magnetization along the +z-axis during the entire experiment, which is achieved by application of the water-selective 90° rf-pulses indicated by curved shapes on the line ^{1}H. (b) Experimental scheme for 3D [^{1}H,^{1}H]-NOESY-[^{15}N,^{1}H]/[^{13}C,^{1}H]-TROSY. Quadrature detection in the ω_1 dimension is achieved by States-TPPI (Marion et al., 1989) applied to the phase ζ_1, which is otherwise set to {x}. The additional PFG, G_P, has an amplitude of 70 G/cm and a duration 2 ms. All other parameters are set as in (a).

The TROSY technique, applied separately to backbone ^{15}N–^{1}H groups (Pervushin et al., 1997, 1998b) and aromatic ^{13}C–^{1}H groups (Pervushin et al., 1998a; Meissner and Sørensen, 1999a, b), relies on spectroscopic means to reduce the T_2 relaxation rate, using the fact that cross-correlated relaxation caused by interference of DD couplings and CSA interactions gives rise to different relaxation rates of the individual multiplet components in heteronuclear systems of two coupled spins $\frac{1}{2}$, I and S. Theory shows that for the ^{15}N–^{1}H fragment of a peptide bond at ^{1}H frequencies near 1 GHz, highly efficient cancellation of transverse relaxation effects within the ^{15}N–^{1}H moiety can be achieved for one of the four multiplet components. For aromatic ^{13}C–^{1}H groups a corresponding effect on one of the ^{13}C doublet components is observed over the entire ^{1}H frequency range from 500 to 900 MHz (Pervushin et al., 1998a). TROSY observes exclusively the narrow multiplet component, for which the residual linewidth is then mainly due to DD interactions with remote hydrogen atoms in the protein. In this paper we combine the basic features of [^{15}N,^{1}H]-TROSY and [^{13}C^R,^{1}H^R]-TROSY in a single measurement, and we show that the TROSY principle can simultaneously also be applied to the observation of the side-chain ^{15}N–^{1}H$_2$ correlations in large proteins.

Methods

A general product operator analysis of the ^{15}N–^{1}H and ^{13}C–^{1}H correlations for standard polarization transfer delays of $\tau = 1/4^{1}J_{HN}$ and $\tau = 1/4^{1}J_{HC}$, respectively, has been presented by Pervushin et al. (1998b) and by Meissner and Sørensen (1999b). In this paper we consider polarization transfers with arbitrary delays τ, and demonstrate that with the use of τ-values in the range $1/4^{1}J_{HC} < \tau < 1/6^{1}J_{HN}$ the experimental scheme of Figure 1a enables simultaneous TROSY-type acquisition of the ^{15}N–^{1}H, ^{13}C^{R}–^{1}H^{R} and ^{15}N–^{1}H$_2$ correlations, with high sensitivity of the individual correlations and with minimal introduction of spectral artifacts.

The first INEPT element (Morris and Freeman, 1979) in Figure 1a is used to excite ^{15}N single quantum coherence in antiphase with respect to the directly attached amide proton, ^{1}H^{N}. For large proteins, transverse relaxation during INEPT transfer may shift the conditions for maximum coherence transfer to τ' values that are shorter than the 'standard optimal value' of $1/4^{1}J_{HN}$ (Cavanagh et al., 1996). With shorter transfer delays τ' the INEPT element can then be employed to simultaneously excite ^{13}C^{R} single-quantum coherence in antiphase with respect to ^{1}H^{R}. Subsequently the ^{15}N as well as the ^{13}C^{R} magnetizations can be used to record the corresponding chemical shifts in TROSY-type manner (Pervushin et al., 1997), with detection by the single transition-to-single transition polarization transfer (ST2-PT) element (Pervushin et al., 1998b). In ST2-PT-based [^{15}N,^{1}H]-TROSY the experimental scheme is commonly tuned to correlate exclusively the ^{15}N transition with the slower transverse relaxation rate to the more slowly relaxing transition in the ^{1}H doublet. In the basis of single transition operators the effects of the INEPT polarization transfer (Morris and Freeman, 1979) and the ST2-PT element (Pervushin et al., 1998b) can thus be interpreted as projections of the initial spin operators representing the Boltzmann steady-state ^{1}H and ^{15}N magnetizations, I_z and S_z, onto the corresponding single-transition operators representing the ^{15}N magnetization, $S_r^{\pm}$ and $S_s^{\pm}$, i.e., $< U'(I_z + S_z)U'^{\dagger}|S_i^{\pm} >$, where $U'^{\dagger}$ is the Hermitian conjugate of U' and i = r,s. In this representation the propagator U' is the product of the unitary operators representing delays and non-selective pulses in the INEPT element given by Equation 1.

$$U' = U^{x}(^{1}H) * U^{2\tau} * U^{y}(^{1}H) * U^{\Psi 1} \quad (1)$$

Subsequently, the operators $S_r^{\pm}$ and $S_s^{\pm}$ can be projected onto the corresponding single-transition operators representing the detectable ^{1}H magnetization, I_r^{-} and I_s^{-} (Glaser et al., 1998), i.e., $<U S_i^{\pm} U^{\dagger}|I_j^{-}>$, where U is the product of the unitary operators in the ST2-PT element (see box in Figure 1a) given by Equation 2, $U^{\dagger}$ is the Hermitian conjugate of U, and i,j = r,s.

$$U = U^{\Psi 2} * U^{2\tau} * U^{x}(^{1}H) * U^{\Psi 4} * U^{2\tau} * U^{x}(^{15}N) \quad (2)$$

In the following, scalar products of the type $<U A_i U^{\dagger}|B_j>$ are represented by the pair of corresponding indices, (z,r,s)/(r,s), and they can be described by the expressions 3–14, where for simplicity $J = {}^{1}J(^{15}N,^{1}H)$ or ${}^{1}J(^{13}C,^{1}H)$.

For the first INEPT step, the polarization transfer for the TROSY and non-TROSY components of the spin S doublet is given by Equations 3 and 4.

$$z/s = 1/2(v + u\, sin(2\pi\tau' J) exp(-2R_{sq}\tau')) \quad (3)$$

$$z/r = 1/2(-v + u\, sin(2\pi\tau' J) exp(-2R_{sq}\tau')) \quad (4)$$

The constant factors u and v reflect the relative magnitudes of the steady-state magnetizations of ^{1}H and ^{15}N, or ^{13}C, respectively, which are determined by the gyromagnetic ratios, the spin–lattice relaxation rates and the delay between individual data recordings (Ernst et al., 1987). For example, in the simulations shown in Figure 1, a–c, we used $v = 0.14$ and $u = 1$ (Pervushin et al., 1998b), $v = 1$ and $u = 1$ (Brutscher et al., 1998; Pervushin et al., 1998a), and $v = 0.07$ and $u = 1$, respectively. R_{sq} is the transverse relaxation rate of the proton antiphase coherences that evolve during the INEPT transfer. For the presentations in Figure 2, R_{sq} has been calculated according to Salzmann et al. (1998) for a rigid spherical molecule with a rotational correlation time of 33 ns, which corresponds to the rotational correlation time of OmpA in DHPC micelles at 30 °C calculated from the backbone $T_1(^{15}N)$ and $T_2(^{15}N)$ relaxation times (unpublished data).

In the 2D [^{15}N,^{1}H]/[^{13}C,^{1}H]-TROSY experiment with an ST2-PT element (Figure 1), the chemical shift evolution during the t_1 period modulates the phase of the signal recorded during t_2, so that two data sets are collected, i.e. P-type and N-type, which result from the $S_i^{-} \rightarrow I_j^{-}$ and $S_i^{+} \rightarrow I_j^{-}$ magnetization transfer pathways, respectively (Cavanagh et al., 1996). Here, the polarization transfer functions for the P-type data set measured with the complete phase cycle of Figure 1a are reported. Identical polarization transfer

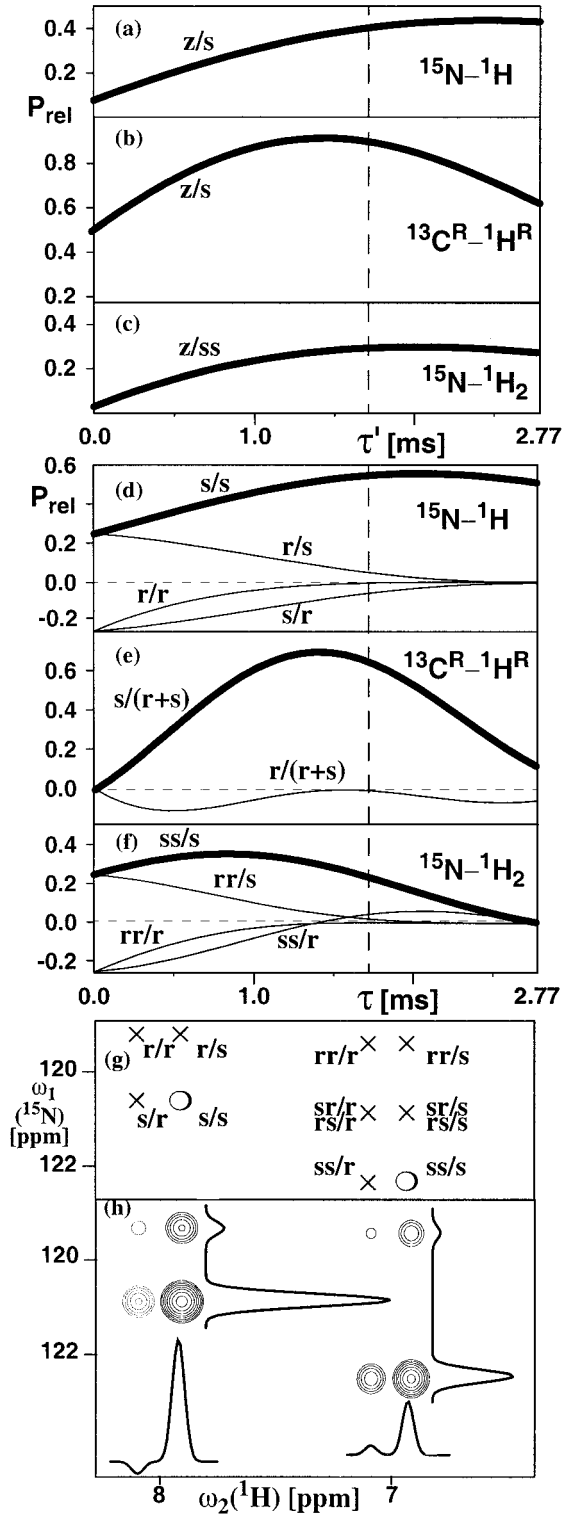

Figure 2. (a)-(c) Plots of the relative extent of polarization transfer for the TROSY component, P_{rel} versus the transfer delay τ' used in the INEPT element of the experimental scheme of Figure 1a. (a) 2D ^{15}N–^{1}H correlation (Equation 3, with $\nu = 0.14$, $u = 1$ and $J = 90$ Hz). (b) 2D ^{13}C–^{1}H correlation (Equation 3, with $\nu = 1$, $u = 1$ and $J = 160$ Hz). (c) 2D ^{15}N–^{1}H$_2$ correlation (Equation 3, with $\nu = 0.07$, $u = 1$ and $J = 90$ Hz). (d)–(f) Plots of P_{rel} versus the transfer delay τ used in the ST2-PT element (box in the experimental scheme of Figure 1a) for all components of the 2D peak fine structure.(d) 2D ^{15}N–^{1}H multiplet components (Equations 5–8). (e) ^{13}C doublet components of the 2D ^{13}C–^{1}H multiplet (Equations 13 and 14). (f) 2D ^{15}N–^{1}H$_2$ multiplet components (Equations 9–12). In (d)–(f) the curves correspond to Equations 5–14, as indicated in the figure, multiplied by $\exp(-4R_{av}\tau)$, and thus describe the time evolution of the magnetizations during the ST2-PT element with inclusion of relaxation. The TROSY component is represented by a thick line. The volumes of the corresponding cross peaks in the 2D ^{15}N–^{1}H and ^{13}C–^{1}H correlation spectra are proportional to both, P_{rel} for the TROSY component in the INEPT step and P_{rel} for the ST2-PT element (see the text for further details). The vertical dashed line indicates the delays $\tau' = \tau = 1.7$ ms, which we propose as a good compromise for experiments designed for simultaneous observation of all three correlations. (g) Scheme showing peak positions for a ^{15}N–^{1}H moiety and a ^{15}N–^{1}H$_2$ moiety, with $^{1}J_{HN} = 90$ Hz, $\tau = 2.77$ ms, ^{15}N chemical shifts of 120 ppm (backbone ^{15}N) and 121 ppm (side-chain ^{15}N), and ^{1}H chemical shifts of 8 ppm (backbone $^{1}H^{N}$), 7 ppm (side chain $^{1}H^{2}$) and 6 ppm (side-chain $^{1}H^{3}$, not shown). The positions of the desired TROSY cross peaks are indicated by circles and the unwanted components of the 2D ^{15}N–^{1}H and ^{15}N–^{1}H$_2$ multiplets by crosses. In (d)–(f), the 2D cross-peak components are identified with the corresponding polarization transfer pathways (Equations 5–14). (h) Simulation of the relative peak intensities in spectrum (g) for a polarization transfer delay $\tau = 1.7$ ms. A contour plot and cross sections along both frequency axes through the TROSY cross peaks are shown. Spin relaxation was not considered in this simulation. Using the program PROSA (Güntert et al., 1992) the spectrum was simulated by Fourier transformation of an interferogram generated with the use of the program NMRSIM (Bruker Inc.), which had been multiplied in the two spectral dimensions with the Gauss–Lorentz window functions $w(t) = \exp(-\pi t 100(1.1 - t/t_{1max}))$ and $w(t) = \exp(-\pi t 100(1.1 - t/t_{2max}))$ (Ernst et al., 1987), with $t_{1max} = 256$ ms and $t_{2max} = 166$ ms, respectively.

functions are obtained for the N-type data set. For P-type and N-type data sets with unbalanced signal intensity, quadrature artifacts would arise. We did not observe such artifacts either in numerical spectral simulations or in experimental measurements, neither for $\tau = 1/4J_{HN}$ nor for $\tau < 1/4^{1}J_{HN}$.

For the ST2-PT element, the polarization transfer for the TROSY and non-TROSY components of the spin *S* to the TROSY and non-TROSY components of the spin *I* is given by the Equations 5–8, which were evaluated with the program POMA (Güntert et al., 1993).

$$s/s = 1/4(1 + sin(2\pi\tau J))^2 \qquad (5)$$

$$r/r = 1/4(1 - sin(2\pi\tau J))^2 \quad (6)$$

$$r/s = 1/4(1 - sin^2(2\pi\tau J)) \quad (7)$$

$$s/r = -1/4(1 - sin^2(2\pi\tau J)) \quad (8)$$

The coherence transfer pathway of Equation 5 results in the desired TROSY cross peak, with narrow linewidths in both the ^{15}N and ^{1}H spectral dimensions due to the constructive use of CSA/DD relaxation interference (Pervushin et al., 1997), and the pathways of Equations 6–8 generate the three unwanted cross-peak components. In the absence of relaxation, a transfer delay $\tau = 1/4J_{HN}$ would completely suppress unwanted cross-talk between broad and narrow transitions. In reality, relaxation-induced imbalance between the different coherence transfer pathways utilized in ST2-PT may give rise to small signals from Equations 7 and 8, even with $\tau = 1/4J_{HN}$ (Rance et al., 1999).

For N–H_2 groups the polarization transfer functions are given by Equations 9–12, where J stands for the average of the $^{1}J_{H1N}$ and $^{1}J_{H2N}$ couplings, and it is assumed that the difference $|^{1}J_{H1N} - ^{1}J_{H2N}|$ is smaller than either the ^{15}N or the $^{1}H^{N}$ linewidths.

$$\begin{aligned} ss/s = {} & 1/4 + cos(2\pi\tau J)/8 + cos(4\pi\tau J)/4 \\ & - cos(6\pi\tau J)/8 + sin(2\pi\tau J)/8 \\ & + sin(4\pi\tau J)/4 + sin(6\pi\tau J)/8 \end{aligned} \quad (9)$$

$$\begin{aligned} rr/r = {} & -(1/4 + cos(2\pi\tau J)/8 + cos(4\pi\tau J)/4 \\ & - cos(6\pi\tau J)/8 - sin(2\pi\tau J)/8 \\ & - sin(4\pi\tau J)/4 - sin(6\pi\tau J)/8) \end{aligned} \quad (10)$$

$$\begin{aligned} rr/s = {} & -(-1/4 + cos(2\pi\tau J)/8 - cos(4\pi\tau J)/4 \\ & - cos(6\pi\tau J)/8 + sin(2\pi\tau J)/8 \\ & - sin(4\pi\tau J)/4 + sin(6\pi\tau J)/8) \end{aligned} \quad (11)$$

$$\begin{aligned} ss/r = {} & (-1/4 + cos(2\pi\tau J)/8 - cos(4\pi\tau J)/4 \\ & - cos(6\pi\tau J)/8 - sin(2\pi\tau J)/8 \\ & + sin(4\pi\tau J)/4 - sin(6\pi\tau J)/8) \end{aligned} \quad (12)$$

The central components of the ^{15}N multiplet, rs/s, rs/r, sr/s and sr/r, are usually not observed in the experimental spectra since they are not excited by the first INEPT element (Morris and Freeman, 1979), and small fractions of these coherences that could possibly be induced by relaxation are further suppressed by the ST2-PT element.

For $^{13}C^{R}$–$^{1}H^{R}$ groups broadband ^{13}C-decoupling is used during the ^{1}H acquisition, resulting in the corresponding transfer functions given by Equations 13 and 14 for the TROSY and non-TROSY cross peaks, respectively, where $J = {}^{1}J(^{13}C,^{1}H)$.

$$s/(r + s) = (sin(2\pi\tau J) + sin^2(2\pi\tau J))/2 \quad (13)$$

$$r/(r + s) = (sin(2\pi\tau J) - sin^2(2\pi\tau J))/2 \quad (14)$$

To properly account for the transverse relaxation rates, the Equations 5 to 14 must be multiplied by $\exp(-4R_{av}\tau)$, where R_{av} is the average of the transverse relaxation rates of the *IS* multiple quantum coherence and the proton antiphase coherences that evolve during the ST2-PT element. R_{av} has been calculated according to Salzmann et al. (1998) and Pervushin et al. (1999) for a rigid spherical molecule with a rotational correlation time of 33 ns. Figure 2 shows that values of 1.5 to 2.0 ms can be used for the τ' and τ delays without significantly compromising the sensitivity for detection of the ^{15}N–^{1}H signal, when compared with the optimal τ' and τ values of 2.7 ms, and that the $^{13}C^{R}$–$^{1}H^{R}$ and ^{15}N–$^{1}H_2$ correlations can then be observed simultaneously with good sensitivity. The model calculations further confirm the well-known fact (Morris and Freeman, 1979) that the short τ delays may cause the appearance of small unwanted cross peaks, in particular r/s and s/r for ^{15}N–^{1}H, and rr/s and ss/r for ^{15}N–$^{1}H_2$ (Figure 2, d and f–h). However, all these 'unwanted' peaks are largely attenuated by destructive DD/CSA interference in one or both spectral dimensions, and are not expected to be observed in [^{15}N,^{1}H]/[^{13}C,^{1}H]-TROSY spectra of particles with size above ca. 30 kDa.

Figure 1b shows the experimental scheme of 3D [^{1}H,^{1}H]-NOESY-[^{15}N,^{1}H]/[^{13}C,^{1}H]-TROSY, where the [^{15}N,^{1}H]/[^{13}C,^{1}H]-TROSY experiment of Figure 1a is used as the heteronuclear correlation element in the previously described TROSY-type heteronuclear-resolved [^{1}H,^{1}H]-NOESY scheme (Pervushin et al., 1999).

Results and discussion

All NMR experiments were performed with the $^{2}H(^{1}H^{R})$,^{13}C,^{15}N-labeled N-terminal 171-residue transmembrane domain of the *E. coli* outer membrane protein A (OmpA) reconstituted in DHPC micelles. The protein concentration was 2 mM in 95%/5% $^{1}H_2O/^{2}H_2O$, containing 150 mM DHPC, 100 mM NaCl and 20 mM phosphate buffer at pH 6.8. This domain forms a membrane-spanning β-barrel (Pautsch and Schulz, 1998). The protein was overexpressed in

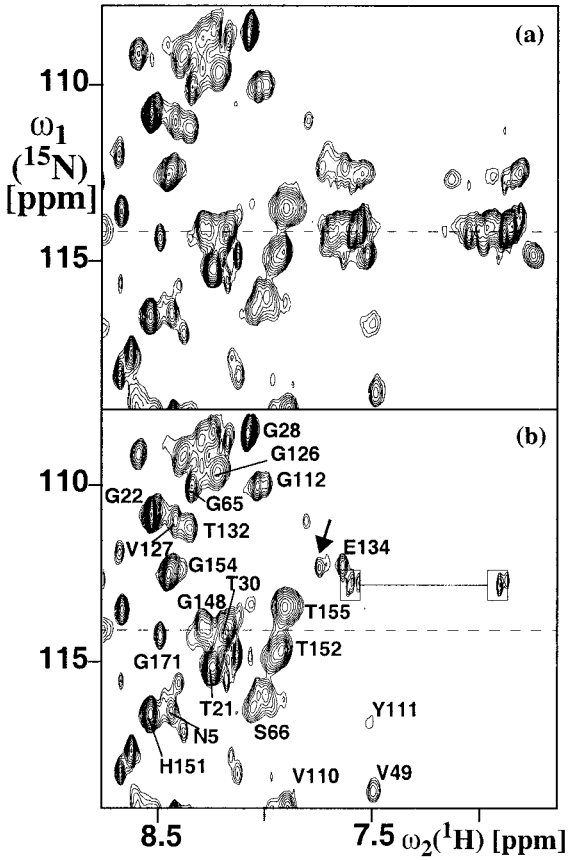

Figure 3. Comparison of two ^{15}N,^{1}H-correlation experiments performed with [^{2}H(^{1}H^{R}),^{15}N,^{13}C]-labeled OmpA solubilized in DHPC micelles in 95% $^{1}H_2O$/5% $^{2}H_2O$ solution (K. Pervushin, C. Fernández and K. Wüthrich, unpublished data) (protein concentration 2 mM, pH = 6.8, T = 30 °C) on a Bruker DRX-750 spectrometer. The contour plots displayed are of a spectral region that contains backbone ^{15}N–^{1}H resonances as well as signals from Asn and Gln side-chain ^{15}N–$^{1}H_2$ groups. (a) 2D [^{15}N,^{1}H]-TROSY spectrum measured with $\tau' = \tau = 1.7$ ms. (b) 2D [^{15}N,^{1}H]-TROSY spectrum measured with $\tau' = \tau = 2.77$ ms. The data size for both spectra was 1024 (t_2) ∗ 300 (t_1) complex points, with $t_{2max} = 102.4$ ms and $t_{1max} = 42$ ms. In (b), resonance assignments are indicated for some backbone ^{15}N–^{1}H cross peaks, using one-letter amino acid symbols and sequence positions. Chemical shifts in ppm are relative to DSS. The horizontal dashed lines identify the locations of the cross sections along ω_2 that are shown in Figure 4. In (b) the two boxes connected by a solid horizontal line show resonances of ^{15}N–^{1}H^{2}H moieties, and an arrow indicates a backbone ^{15}N–^{1}H cross peak which is masked by the strong ^{15}N–$^{1}H_2$ cross peaks in spectrum (a).

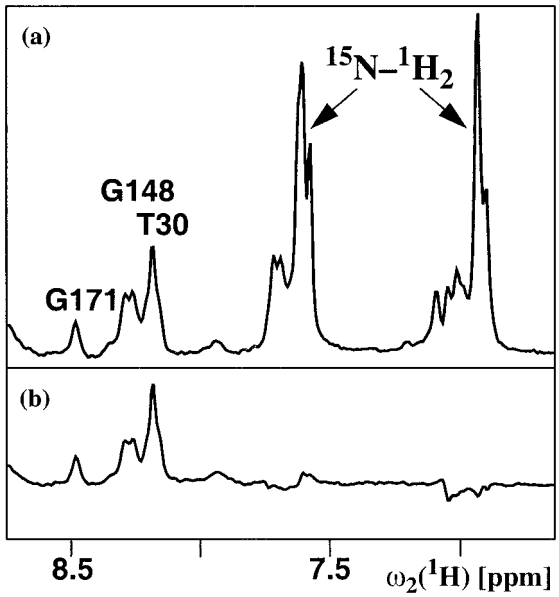

Figure 4. Cross sections parallel to the ω_2(^{1}H) axis at the positions of the broken horizontal lines through the 2D[^{15}N,^{1}H]-TROSY spectra of OmpA/DHPC in Figure 3. (a) [^{15}N,^{1}H]-TROSY recorded with $\tau' = \tau = 1.7$ ms; (b) [^{1}H,^{15}N]-TROSY recorded with $\tau' = \tau = 2.77$ ms. Sequence-specific assignments for some backbone ^{15}N–^{1}H resonances are indicated as in Figure 3.

inclusion bodies and renatured in the presence of the detergent, according to Pautsch et al. (1999).

The use of the combined [^{15}N,^{1}H]/[^{13}C,^{1}H]-TROSY approach for NMR experiments with large proteins to establish ^{15}N–^{1}H correlations in the protein backbone and the side chains of Arg, Asn, Gln and Trp, and ^{13}C–^{1}H correlations in the aromatic rings of ^{2}H(^{1}H^{R}),^{13}C,^{15}N-labeled proteins is first illustrated by comparison of the 2D [^{15}N,^{1}H]-TROSY subspectra measured with, respectively, $\tau = 1/4^{1}J_{HN}$, which corresponds to the conventional TROSY experiment (Pervushin et al., 1998b), and the presently proposed delay of $\tau = 1.7$ ms. A small region from these two [^{15}N,^{1}H]-TROSY spectra, which contains also resonances of side-chain NH_2 groups, is compared in Figure 3. The spectra were measured at 30 °C, where the correlation time for OmpA in DHPC micelles was estimated from T_1(^{15}N) and T_2(^{15}N) measurements to be $\tau_c = 33$ ns. With $\tau = \tau' = 1.7$ ms the backbone ^{15}N–^{1}H cross peaks as well as numerous side-chain ^{15}N–$^{1}H_2$ correlations are observed. A quantitative comparison of the two measurements is afforded by the cross-sections along ω_2(^{1}H) taken at the ^{15}N chemical shift indicated in Figure 3 by a dashed horizontal line (Figure 4). The use of the shorter delay τ thus yields similar or even slightly better sensitivity for the ^{15}N–^{1}H correlations, and provides additional ^{15}N–$^{1}H_2$ correlations. Since the strong ^{15}N–$^{1}H_2$ cross peaks could obscure some of the backbone ^{15}N–^{1}H resonances, such as the one marked by an arrow in Figure 3b, it may be desir-

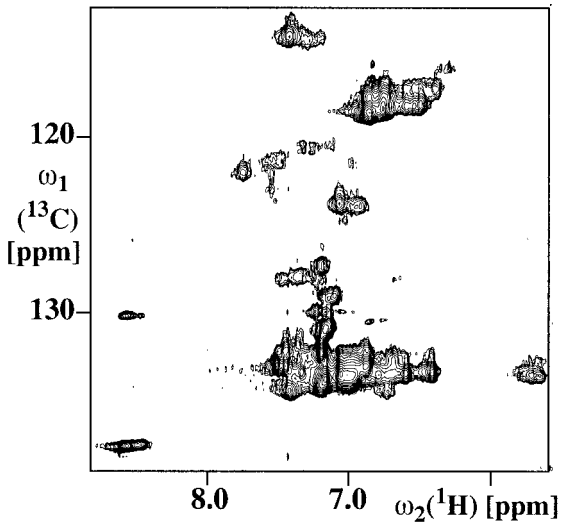

Figure 5. 2D [$^{13}C^{R}$,$^{1}H^{R}$]-TROSY subspectrum of [$^{2}H(^{1}H^{R})$, ^{15}N,^{13}C]-labeled OmpA/DHPC extracted from the same data set as the [^{1}H, ^{15}N]-TROSY subspectrum of Figure 3a. Chemical shifts in ppm are relative to DSS.

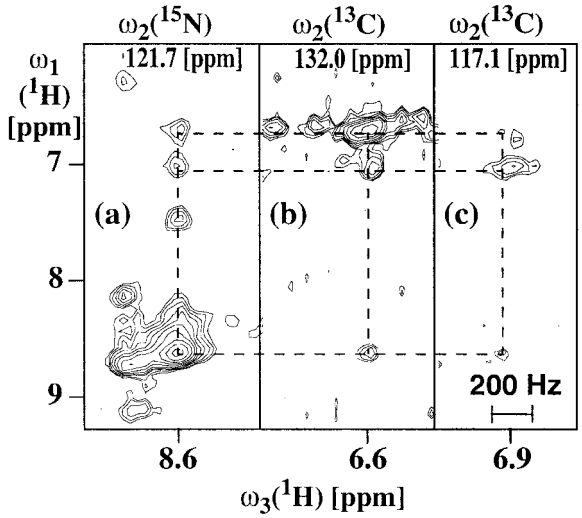

Figure 6. 3D [^{1}H,^{1}H]-NOESY-[^{15}N,^{1}H]/[^{13}C,^{1}H]-TROSY experiment recorded on a Bruker DRX-750 spectrometer with the same sample of OmpA/DHPC as in Figure 3, using the experimental scheme of Figure 1b. $80(t_1) * 35(t_2) * 1024(t_3)$ complex points were accumulated, with t_{1max} = 8.8 ms, t_{2max} = 15.3 ms and t_{3max} = 102.4 ms. Eight scans per increment were acquired, resulting in a measuring time of 50 h. Contour plots of ($\omega_1(^{1}H)$, $\omega_3(^{1}H)$)-strips are shown. (a) ^{15}N-resolved 3D [^{1}H,^{1}H]-NOESY subspectrum at $\omega_2(^{15}N)$ = 121.7 ppm; (b) and (c) $^{13}C^{R}$-resolved 3D [^{1}H,^{1}H]-NOESY subspectrum at $\omega_2(^{13}C)$ = 132.0 ppm and at $\omega_2(^{13}C)$ = 117.1 ppm, respectively. The NOESY diagonal peaks and cross peaks connected with dashed lines have been tentatively assigned to Tyr94.

able for complete spectral assignment and extraction of structural constraints to record two spectra with and without ^{15}N–$^{1}H_2$ correlations, respectively (Figures 3 and 4).

As a second illustration, the 2D [^{13}C,^{1}H]-TROSY subspectrum obtained from the experiment of Figure 1a, which correlates $^{13}C^{R}$ and $^{1}H^{R}$ resonances in the aromatic rings of OmpA/DHPC, is shown in Figure 5. Because of the small CSA values of aromatic protons, ^{13}C broadband decoupling is applied during signal acquisition (Pervushin et al., 1998a; Meissner and Sørensen, 1999a,b), so that TROSY is used only for suppression of the unwanted component of the ^{13}C doublet (Figure 2b). The experimental scheme of Figure 1a enables separate optimization of the maximal ^{15}N and ^{13}C chemical shift evolution delays, t^{N}_{1max} and t^{C}_{1max}. The t^{N}_{1max} value is chosen so as to provide the desired spectral resolution along the $\omega_1(^{15}N)$ dimension. The t^{C}_{1max} value is adjusted to $1/2^{1}J_{CC}$ (see caption to Figure 1 for details) in order to prevent splitting of the ^{13}C–^{1}H resonances along the $\omega_1(^{13}C)$ dimension due to the $^{1}J_{CC}$ couplings (∼55 Hz). During the ensuing delay of duration $t^{N}_{1} - t^{C}_{1}$ between the Ψ_1 and ϕ_1 pulses (Figure 1a), the ^{13}C magnetization is stored in the form of slowly relaxing two-spin order (Canet, 1989).

For OmpA/DHPC only very small spectral intensity was observed at the positions of the unwanted components of the ^{15}N–^{1}H and $^{13}C^{R}$–$^{1}H^{R}$ multiplets. This can readily be rationalized from the simulations in Figure 2, even though these did not consider transverse relaxation during the ST2-PT element. For $\tau = \tau' = 1.7$ ms the r/s, s/r, rr/s and ss/r ^{15}N–^{1}H peaks show up with about 10% of the volume of the desired TROSY cross peak, and negligibly small volumes result for the ^{15}N–^{1}H r/r and rr/r peaks, and the $^{13}C^{R}$–$^{1}H^{R}$ r/(r+s) peak (Figure 2). In the actual experiment, the unwanted cross peaks are further broadened in one or both spectral dimensions by destructive DD/CSA interference, so that the intensities of the unwanted peaks can be expected to be below 3% of the TROSY cross-peak intensities for particles of the size of OmpA/DHPC.

The use of [^{15}N,^{1}H]/[^{13}C,^{1}H]-TROSY as the heteronuclear correlation element in 3D heteronuclear-resolved NOESY (Figures 1b and 6) can yield improved efficiency as well as novel information. Since several days of accumulation time are typically used to record 3D heteronuclear-resolved NOESY spectra of macromolecular systems (Wider, 1998), the simultaneous acquisition of the ^{15}N-resolved and ^{13}C-

resolved data sets can economize substantial amounts of instrument time. The NOE cross peaks between backbone amide protons and side-chain ^{15}N–$^{1}H_2$ groups yield novel, additional structural constraints, and since the ^{13}C-resolved and ^{15}N-resolved NOESY-TROSY spectra are obtained in an interleaved manner, more reliable [$^{1}H^{N}$,$^{1}H^{R}$]-NOE connectivities can be established based on matching the cross-peak chemical shifts in the two subspectra (Figure 6).

Conclusions

Use of short transfer delays τ and τ' in the experiments of Figure 1 provides an avenue for observing backbone ^{15}N–^{1}H correlations with near-optimal sensitivity under conditions that enable simultaneous observation of the previously TROSY-inaccessible side-chain ^{15}N–$^{1}H_2$ correlations. Furthermore, taking advantage of the ^{2}H isotope labeling pattern achieved when a recombinant protein is produced with 99% $^{2}H_2O$ and u-[^{1}H,^{13}C]-glucose (Gardner and Kay, 1998), the aromatic $^{13}C^{R}$–$^{1}H^{R}$ correlations are also obtained. The experimental schemes of Figure 1 also preserve the tricks of the trade used in conventional TROSY, such as echo–anti-echo quadrature detection (Kay et al., 1992), 'water-flip-back' (Piotto et al., 1992; Grzesiek and Bax, 1993), and the use of the Boltzmann steady-state ^{15}N and ^{13}C magnetizations to increase sensitivity (Pervushin et al., 1998a,b). We recommend in particular the use of the scheme of Figure 1a as a building block in more complex NMR experiments with particle sizes >30 kDa (see Figure 1b).

Acknowledgements

Financial support was obtained from the Schweizerischer Nationalfonds (project 31.49047.96) and the Bundesamt für Bildung und Wissenschaft (Nr. 97.0593) as part of an EU Biomed concerted action (Nr. BMH4-CT 97-2641). We thank Prof. G. Schultz for his kind gift of the OmpA(1–171) expression plasmid.

References

Boelens, R., Burgering, M., Fogh, R.H. and Kaptein, R. (1994) *J. Biomol. NMR*, **4**, 201–213.

Brutscher, B., Boisbouvier, J., Pardi, A., Marion, D. and Simorre, J.P. (1998) *J. Am. Chem. Soc.*, **120**, 11845–11851.

Canet, D. (1989) *Prog. NMR Spectrosc.*, **21**, 237–291.

Cavanagh, J., Fairbrother, W.J., Palmer, A.G. and Skelton, N.J. (1996) *Protein NMR Spectroscopy: Principles and Practice*, Academic Press, New York, NY, p. 247.

Ernst, R.R., Bodenhausen, G. and Wokaun, A. (1987) *The Principles of Nuclear Magnetic Resonance in One and Two Dimensions*, Clarendon, Oxford.

Farmer, B.T. (1991) *J. Magn. Reson.*, **93**, 635–641.

Farmer, B.T. and Mueller, L. (1994) *J. Biomol. NMR*, **4**, 673–687.

Gardner, K.H. and Kay, L.E. (1998) *Annu. Rev. Biophys. Biomol. Struct.*, **27**, 357–406.

Geen, H. and Freeman, R. (1991) *J. Magn. Reson.*, **93**, 93–141.

Glaser, S.J., Schulte-Herbruggen, T., Sieveking, M., Schedletzky, O., Nielsen, N.C., Sørensen, O.W. and Griesinger, C. (1998) *Science*, **280**, 421–424.

Grzesiek, S. and Bax, A. (1993) *J. Am. Chem. Soc.*, **115**, 12593–12594.

Güntert, P., Dötsch, V., Wider, G. and Wüthrich, K. (1992) *J. Biomol. NMR*, **2**, 619–629.

Güntert, P., Schaefer, N., Otting, G. and Wüthrich, K. (1993) *J. Magn. Reson.*, **A101**, 103–105.

Kay, L.E., Keifer, P. and Saarinen, T. (1992) *J. Am. Chem. Soc.*, **114**, 10663–10665.

Marion, D., Ikura, M., Tschudin, R. and Bax, A. (1989) *J. Magn. Reson.*, **85**, 393–399.

Meissner, A. and Sørensen, O.W. (1999a) *J. Magn. Reson.*, **139**, 447–450.

Meissner, A. and Sørensen, O.W. (1999b) *J. Magn. Reson.*, **139**, 439–442.

Morris, G.A. and Freeman, R. (1979) *J. Am. Chem. Soc.*, **101**, 760–762.

Pascal, S.M., Muhandiram, D.R., Yamazaki, T., Forman-Kay, J.D. and Kay, L.E. (1994) *J. Magn. Reson.*, **B103**, 197–201.

Pautsch, A. and Schulz, G.E. (1998) *Nat. Struct. Biol.*, **5**, 1013–1017.

Pautsch, A., Vogt, J., Model, K., Siebold, C. and Schulz, G.E. (1999) *Proteins*, **34**, 167–172.

Pervushin, K., Riek, R., Wider, G. and Wüthrich, K. (1997) *Proc. Natl. Acad. Sci. USA*, **94**, 12366–12371.

Pervushin, K., Riek, R., Wider, G. and Wüthrich, K. (1998a) *J. Am. Chem. Soc.*, **120**, 6394–6400.

Pervushin, K., Wider, G. and Wüthrich, K. (1998b) *J. Biomol. NMR*, **12**, 345–348.

Pervushin, K., Wider, G., Riek, R. and Wüthrich, K. (1999) *Proc. Natl. Acad. Sci. USA*, **96**, 9607–9612.

Piotto, M., Saudek, V. and Sklenar, V. (1992) *J. Biomol. NMR*, **2**, 661–665.

Rance, M., Loria, J.P. and Palmer, A.G. (1999) *J. Magn. Reson.*, **136**, 92–101.

Salzmann, M., Pervushin, K., Wider, G., Senn, H. and Wüthrich, K. (1998) *Proc. Natl. Acad. Sci. USA*, **95**, 13585–13590.

Sattler, M., Maurer, M., Schleucher, J. and Griesinger, C. (1995) *J. Biomol. NMR*, **5**, 97–102.

Slijper, M., Kaptein, R. and Boelens, R. (1996) *J. Magn. Reson.*, **B111**, 199–203.

Wider, G. (1998) *Prog. NMR Spectrosc.*, **32**, 193–275.